Applied Biological Research 27(2): 244-255; (2025)
DOI: 10.48165/abr.2025.27.01.24

BACTERIAL EXOPOLYSACCHARIDE-MEDIATED GREEN SYNTHESIS OF IRON OXIDE NANOPARTICLE AND ITS EFFECT ON BACTERIAL BIOFILM

Riyanki Das[1,5], Sukhen Bhowmik[2], Debjani Bhowmik[3], Abhijit Bhattacharya[4], L. Robindo Singh[1], and Manash C. Das[5*]

[1]*Department of Nanotechnology, North Eastern Hill University, Shillong - 793 022, Meghalaya (India)*
[2]*Department of Chemistry, Tripura University, Suryamaninagar - 799 022, Tripura (India)*
[3]*Department of Computer Science & Engineering, Faculty of Science & Technology, ICFAI University, Kamalghat - 799 210, Tripura (India)*
[4]*Department of Chemistry, Bir Bikram Memorial College, College Tilla - 799 004, Tripura (India)*
[5]*Microbial Biotechnology Lab, Department of Medical Laboratory Technology, Women's Polytechnic, Hapania - 799 130, Tripura (India)*
*****e-mail: *manashmbt@gmail.com*

(Received 31 December, 2024; accepted 16 June, 2025)

ABSTRACT

Biofilm provides armor to the planktonic bacteria as a strategy to develop tolerance against antibacterial drugs. *Escherichia coli* and *Bacillus subtilis* are the major biofilm forming bacteria who synthesize exopolysaccharide matrix upon which planktonic cells embed themselves to form biofilm. In present work iron oxide nanoparticles (NPs) were synthesized using EPS and their antibiofilm activity against these bacteria were assessed. Nanoparticles GFNB (*B. subtilis* EPS mediated) and GFNE (*E. coli* EPS mediated) were synthesized by EPS mediated-hydrothermal method. Nanoparticles were characterized by UV, FTIR, XRD, TEM and FTIR techniques. Through TEM, iron-oxide NPs were found crystalline having < 5 nm and < 2nm size in case of GFNB and GFNE, respectively. Iron-oxide NPs inhibited planktonic bacterial growth at 1.3 and 3.2 µg mL^{-1} for GFNB and GFNE, respectively, against *E. coli* and at 3.2 and 4.2 µg mL^{-1} for GFNB and GFNE, respectively, against *B. subtilis*. NPs exhibited inhibition on biofilm formation and dispersion of sessile cells at sub-inhibitory concentrations. The study explored a mechanism to green synthesize iron-oxide NPs utilizing bacterial EPS through hydrothermal method which exhibit antibiofilm property.

Keywords: Biofilm, dispersion, characterisation, iron oxide nanoparticle, TEM

INTRODUCTION

Biofilms are microbial consortia of surface attached cells confined within extra-cellular polymeric substances secreted by them. In planktonic form, bacteria exist as a free living state, whereas in biofilm they grow closely attached to each other (Mahto and Das, 2022; Li *et al*., 2023). About 80% infections in animals reportedly are of biofilm origin, whereas around 61% human biofilm infections are from zoonotic origin (Nandanwar *et al.,* 2014). Microbial biofilms often exhibit numerous deleterious effects in agriculture, clinical, industrial environments and veterinary medicine especially in livestock which leads to severe economic loss (Armbruster *et al*., 2019; Erega *et al*., 2021). However, very little attention has been given to animal biofilm infections over past few years.

B. subtilis is one of the major pathogen which causes infection at wound cuts in horses as well as mastitis in domestic animals. Microbial biofilms show multifactorial tolerance towards several antibiotics (Raeispour and Ranjbar, 2018; Kobayashi *et al*., 2021; Edet *et al*., 2023). *B. subtilis* and *E. coli* from animal wound infections reportedly have developed tolerance to several antibiotics such as cloxacillin, erythromycin, cepfodoxime, streptomycin, tetracyclins (Kibret *et al.,* 2011). The emergence of antibiotic-tolerant bacterial strains has resulted into the reduced affectivity of presently available drugs in market (Reddy *et al*., 2014; Parulekar *et al*., 2019; Rashid *et al*., 2021). This trend of antimicrobial tolerance along with toxicity of known antibiotics emphasize to explore some alternative antimicrobial and antibiofilm approaches.

Nanotechnology is an emerging field of science where mechanical, physicochemical and bioactive properties are manipulated at nanoscale level (Li *et al*., 2017). Nanotechnology based antimicrobial strategy involves metal, metal oxide nanoparticles and metal-oxide nanocomposites. Among these, doped or composite nanomaterials reportedly possess significant antimicrobial activity due to synergism of their constitutive individual elemental form. Metallic silver nanoparticle (NP) is commonly known for its antibacterial activity against several Gram positive and Gram negative bacteria (More *et al.,* 2023). Iron oxide NPs also have a wide array of uses in biology and medicine due to their biocompatibility and less toxicity (Pandi *et al*., 2019). Copper when doped with iron oxide NPs, increases its antibacterial activity as compared to the undoped iron oxide NPs (Bustamante-Torres *et al*., 2022). Recently, silver-zinc oxide nanostructures have been exploited for their antibacterial potential against *Streptococcus mutans* and *Bacillus subtilis* (Reddy *et al*., 2014; Malhotra *et al*., 2023). There are very few reports about the effect of iron oxide NPs on planktonic bacteria (Saravanakumar *et al.,* 2022). The present study explored such effect on planktonic and biofilm forming bacteria. The study was aimed to synthesize iron oxide NPs using bacterial EPS by hydrothermal technique and also to explore the effect of synthesized NPs on bacterial aggregation in biofilm formation and dispersion of sessile bacteria from biofilm.

MATERIALS AND METHODS

Collection of ground water and separation of crude iron

Ground water was collected through tube well attached pump and stored for 2-3 days at room temperature. Suspended iron which had settled down at the bottom of bucket was separated. After settling of iron aggregates, water samples containing dissolved iron were collected for the synthesis of nanoparticles.

Synthesis of iron oxide nanoparicles

Bacterial exopolysaccharide (EPS)-mediated iron oxide nanoparticles were prepared by green synthesis (Gobinda *et al.,* 2023). EPS (5 mg) was dissolved in 10 mL ground water (GW), vigorously blended at room temperature for 10-15 min and stirred well at 120°C for 2-3 h to uniformly blend EPS in ground water. The solution was allowed to settle at 4°C for 2-3 h. The solution was centrifuged (Remi CM-8 Plus) at 6000 rpm for 5 min at room temperature and the supernatant collected which was further centrifuged at 8000 rpm for 3-5 min. The collected supernatant was again centrifuged at 12000 rpm for 10 min. Fine nanoparticles deposited at the base of tube were washed at 12000 rpm for 3-5 cycles (Yadwade *et al*., 2021; Jacinto *et al*., 2021).

Characterization of nanoparticles

UV-visible spectroscopy: Absorbance of synthesized compounds were observed under UV spectrophotometer (Labindia UV 3200) starting from 400 nm to 800 nm and continuous absorbance were recorded for 10 min and plotted (Poulose *et al*., 2014).

FTIR spectroscopy: FTIR spectra of synthesized nanostructures were determined by FTIR spectrophoto-

meter (JASCO FT/IR-6100). The analyses were performed with KBr pellets and recorded in range of 400-4000 cm^{-1}. Different modes of vibrations were observed and assigned to determine the various functional groups in sample (Mudunkotuwa *et al*., 2014).

X-ray diffraction analysis: Powdered form of synthesized nanostructures was subjected to XRD analysis (D8, ADVANCE, BRUKER, Axs). X-ray diffractometer (Agilent Gemini) was operated at a current of 40 mA with 40 kV voltage and Cu.Kα radiation of wavelength 1.5406A°. The sample was scanned in the range of 2θ from 20° to 80° with 0.04°/s (Bunjes *et al*., 2007; Tetyczka *et al*., 2019).

Transmission electron microscopy: The surface topography, shape and size of nanoparticles were determined by TEM (JEM-2100, 200 kV, Jeol) Nanoparticles were dissolved in ethanol and sonicated in the bath sonicator for 15 min. A drop of sample was put onto the carbon coated copper grid and allowed to dry. The grid was then fixed onto the holder and observed under TEM (JEM-2100, 200 kV, Jeol) (Petrushevska *et al*., 2021).

Antibacterial and antibiofilm activity

Microbial strains and growth media: *E. coli* MTCC 443 and *B. subtilis* MTCC 441 were procured from IMTECH, Chandigarh (India) and cultured in Lauria Bertoni broth (LB) medium (Nagarajan *et al.*, 2010; Nagao *et al.*, 2023). Initially bacteria were streaked from a -80°C glycerol stock onto LB agar plate for activation and a fresh single colony was then inoculated into 25 mL medium and incubated at 37°C for 24 h. The 10^6 CFU mL^{-1} bacterial cell suspensions were used in all the subsequent experiments (Das *et al*., 2022).

Antimicrobial susceptibility testing: Disc diffusion method using the Bauer-Kirby technique was employed for determination of zone of microbial growth inhibition as per recommendation of National Committee for Clinical Laboratory Standards (Traub *et al.*, 1998). The extent of susceptibility was expressed as zone of inhibition. Minimum inhibitory concentration (MIC) of NPs against *E. coli* MTCC 443 and *B. subtilis* MTCC 441 were determined using a standard broth micro-dilution assay using NPs from 0.1 to 100 µg mL^{-1} with distribution at every 0.01 µg mL^{-1} were assayed for their effect on planktonic bacterial growth (Das *et al*., 2022).

Evaluation of bacterial biofilm forming capability: For evaluation of biofilm forming ability, *E. coli* MTCC 443 and *B. subtilis* MTCC 441 were grown in 96-well plate containing LB and incubated at 37°C for 48 h. Wells were then washed three times with sterile phosphate buffer saline (PBS) and stained for 10 min with 0.1% (v/v) crystal violet (CV) for *E. coli* and safranin for *B. subtilis*. The excess stains were removed by washing with sterile PBS and dried overnight at 37°C. Stain adherent with bacteria were re-dissolved in dimethyl sulphoxide (DMSO) and absorbance recorded at 570 and 492 nm, respectively (Garza-Cervantes *et al*., 2019; Swidan *et al*., 2022; Miškovská *et al*., 2022).

Antibiofilm activity of synthesized NPs: To determine interference of biofilm formation upon treatment with NPs, bacteria were incubated with sub-MIC doses (0.8, and 0.325 µg mL^{-1} against *E. coli* and 1.05, and 0.8 µg mL^{-1} against *B. subtilis*) of NPs and standard antibiotic streptomycin. Wells (treated and untreated) were then washed and stained as per the biofilm forming assay (Das *et al*., 2022). Absorbance were measured at 570 and 492 nm, respectively (Swidan *et al*., 2022; Miškovská *et al*., 2022; Garza-Cervantes *et al*., 2019). The biofilm inhibition (%) in all treated wells with respect to untreated controls was determined using the following formula:

$$\text{Biofilm inhibition (\%)} = \frac{\text{OD of treated sample} - \text{OD of untreated control}}{\text{OD of untreated control}} \text{ x } 100$$

Estimation of biofilm protein concentration

To estimate total extractable biofilm protein, the bacteria were inoculated into sterile 96-well plate and incubated at 37°C for 48 h with or without sub-MIC doses of NPs. Planktonic cells were removed, following that the adhered biofilm cells were washed gently with sterile PBS and boiled for 30 min in 5 mL 0.5 N NaOH (Himedia, India). The cell suspensions were centrifuged at 10000 rpm for 5 min

and the resulting supernatant was collected and protein concentration determined as per Lowry's method (Das *et al*., 2022).

$$\text{Total extractable biofilm protein (\%)} = \frac{\text{OD of treated sample} - \text{OD of untreated control}}{\text{OD of untreated control}} \text{ x } 100$$

Estimation of bacterial EPS

Bacteria were allowed to grow into biofilm in 24-well polystyrene plate in presence and absence of sub-MIC dose (0.80, and 0.325 µg mL^{-1} against *E. coli* and 1.05, and 0.8 µg mL^{-1} against *B. subtilis*) of NPs for 48 h at 37°C. EPS were extracted from polystyrene plate as per Das *et al*. (2022) with minor modification. Briefly, biofilm from plate surface were recovered by scrapping thoroughly in sterile water. This biofilm suspension was centrifuged at 10,000 rpm for 20 min at 4°C and the supernatants were collected. Pellets were mixed with 500 µL of 10 mM EDTA, vortexed for 15 min and re-centrifuged at 10000 rpm for 20 min at 4°C to extract cell-bound exo-polysaccharides. Collected supernatant was mixed with previous supernatant. Pooled supernatant was then mixed with 3 volume of chilled absolute ethanol and centrifuged at 10,000 rpm for 20 min at 4°C. The pellet containing sugar from EPS was dissolved in sterile water and measured by phenol sulphuric acid method (Scala *et al*., 2019; Das *et al*., 2022).

$$\text{Inhibition of EPS quantity (\%)} = \frac{\text{OD of untreated sample} - \text{OD of treated sample}}{\text{OD of untreated sample}} \text{ x } 100$$

Microbial adherence on glass surface by fluorescence microscopy

To observe the effect of NPs and streptomycin on biofilm formation over the glass surface, *E. coli* MTCC 443 and *B. subtilis* MTCC 441 (10^6 CFU mL^{-1} bacterial cell suspensions) were allowed to grow on glass cover slips placed in 35 x 10 mm petridish containing LB. Bacterial cells were then treated with selective sub-MIC doses of NPs and streptomycin followed by incubation at 37°C for 48 h. After incubation, cover slips were gently collected from each petri-dish, washed with sterile 1X PBS and stained with acridine orange (4 µg mL^{-1}) for 15 min in dark. The live cells in biofilm form attached on glass surface were observed under the fluorescence microscope (Leica DM 4000B, Germany). Images were captured from 20 different fields from a single cover slip (Das *et al*., 2022).

Motility analysis of E. coli and B. subtilis

Sliding motility of *E. coli* and *B. subtilis* were tested through their ability to spread on LB soft agar media (Himedia, India) containing 2.4 g L^{-1} agar in 35 x 10 mm petridish. Briefly, aliquot bacteria (10^6 CFU mL^{-1}) either treated or untreated with sub-MIC dose of NPs were spot inoculated in the centre of plate and dried for 20 min at room temperature. The plates were then incubated at 37°C for 48 h. Colony growth expansions from the point of inoculation were recorded (Das *et al*., 2022).

Statistical analysis

All the biological experiments were performed in triplicate and data were recorded as the mean ± standard deviation. Significant values were calculated using one-way ANOVA t-test (Das *et al.,* 2022) and significance determined as P value< 0.01 (*), P value< 0.001 (**) and P value< 0.0001 (***).

RESULTS AND DISCUSSION

Both nanoparticles showed absorption peaks in UV spectrum (< 300 nm). *Bacillus subtilis* EPS mediated-GFNB showed maximum absorbance (λ_{max}) at 280 nm and *Escherichia coli* EPS mediated-GFNE showed λ_{max} at 290 nm [Fig. 1A(i)]. This signifies that yellow reddish colour dissolved iron was converted to colourless nanoparticles. The compound GFNB had more hyperchromism than that of compound GFNE. The compound GFNB has slightly more red shift than compound GFNE. Peaks of IR frequencies (cm^{-1}) produced by the compound GFNB were observed at 3413 (O-), 2827(sp^2-), 2264 (C≡C), 1640 (= , =O), 1518 (-O), 1172 (-) [Fig. 1A(ii)] and peaks of IR frequencies (cm^{-1})

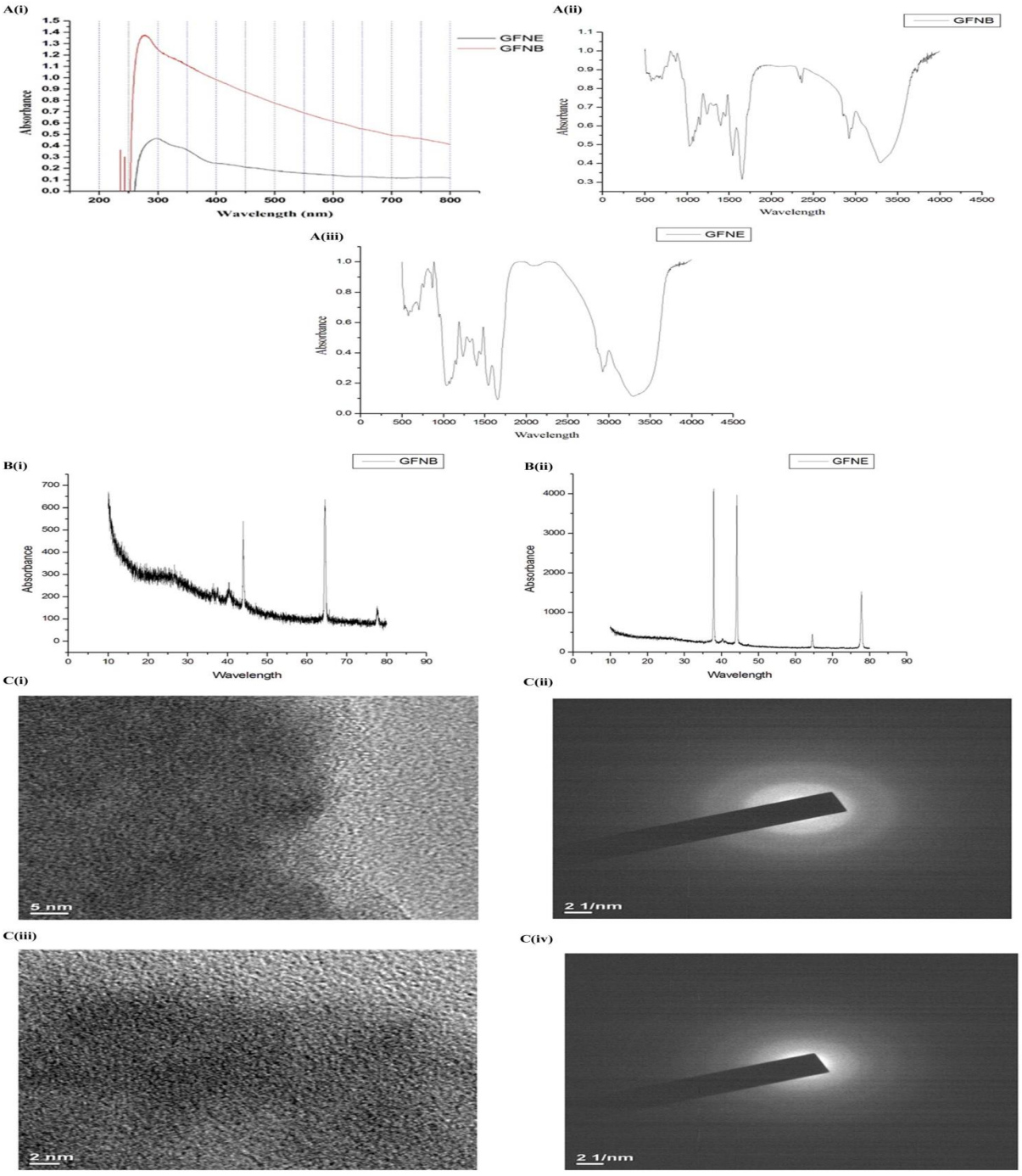

Fig. 1: Absorption spectrum of GFNB and GFNE in UV range [A(i)], IR absorption spectrum of GFNB [A(ii)] and GFNE [A(iii)]. XRD pattern explaining the peaks observed in GFNB [B(i)] and GFNE [B(ii)] are shown. Furthermore, TEM and SAED analysis of GFNB are shown in [C(i)], and [C(ii)] and those of GFNE in [C(iii)], and [C(iv)] respectively.

produced by the compound GFNE were observed at 3319 (O-), 2874(sp^2-), 1676 (=, =O), 1143 (-) [Fig. 1A(iii)]. XRD pattern of synthesized nanoparticles showed two peaks for GFNB at 2θ at 44.100 and 64.050 [Fig. 1 B(i)] corresponding to (200) and (220) planes, respectively. GFNE showed four peaks at 2θ at 38.15, 44.100, 64.050 and 78.120 [Fig. 1 B(ii)] corresponding to (111), (200), (220) and

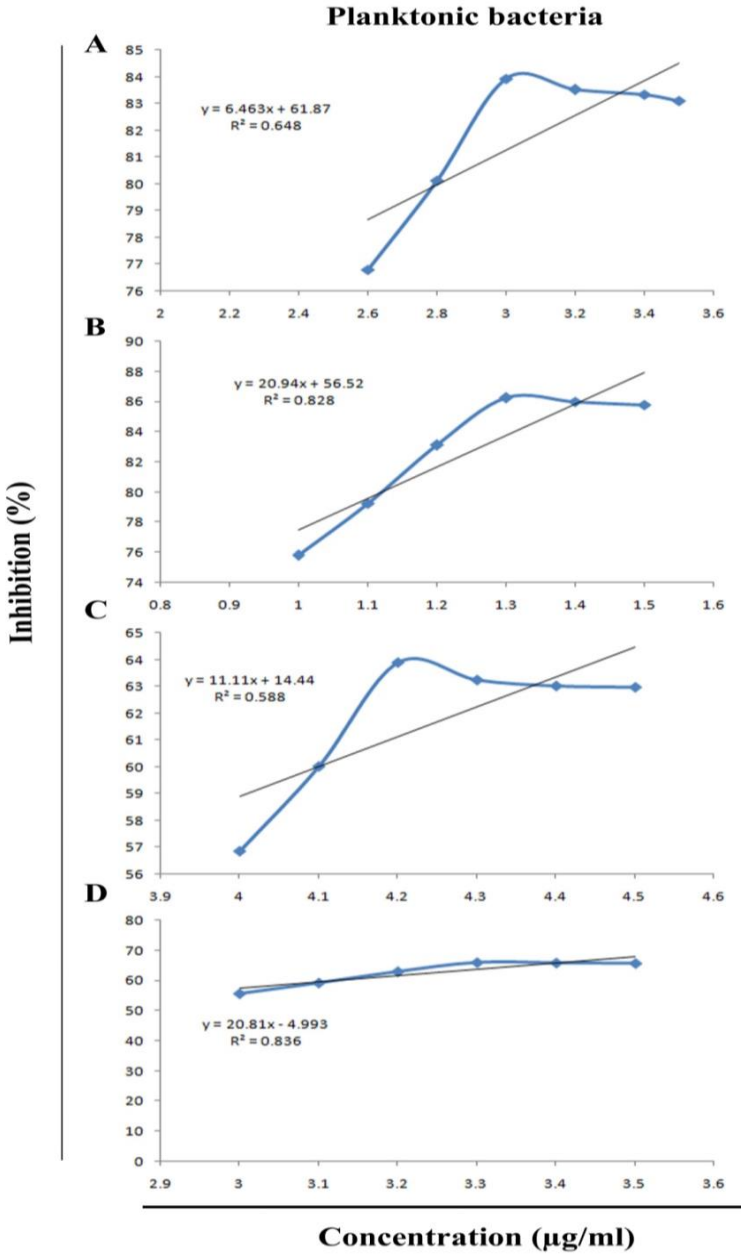

Fig. 2: Antibacterial effect of GFNE [2A], GFNB [2B] against *E. coli* and GFNE [2C], GFNB [2D] against *B. subtilis* are shown here. R^2 value shows the linearity of curve to express significance of percent inhibition or percent dispersion

(335) planes, respectively. These indicate the crystalline nature of sample, and through standard JCPDS data file No. 82-1533 (Qin *et al.*, 2022) confirms that nanocrystals have face-centred cubic (FCC) structure. To obtain TEM image of the prepared NPs, JEM-2100, JEOL instrument was used which worked at 200 kV of accelerating voltage. The synthesized nanoparticles GFNB and GFNE were spherical with size < 5 nm [Fig. 1C(i)] and < 2 nm [Fig. 1C (iii)], respectively. Further, the sharp bright rings and spots in SAED pattern [Fig. 1C(ii), (iv)] were observed which confirm the crystallinity of synthesized nanocrystals whereas GFNB showed more crystalline than GFNE nanoparticles.

A series of concentrations starting from 0.1 to 100 µg mL^{-1}, with distribution at every 0.01 µg mL^{-1}, were assayed for their effect on planktonic bacterial growth. The concentration showing maximum growth inhibition was considered as minimum growth inhibitory concentration with maximum inhibitory effect. The iron oxide NPs showed maximum growth inhibition of planktonic bacteria at 3.2 µg mL^{-1} (83.51%) and 1.3 µg mL^{-1} (86.25%) by GFNE [Fig. 2A] and GFNB [Fig. 2B], respectively, against *E. coli*. In case of planktonic *B. subtilis* GFNE and GFNB exhibited

Table 1: Effect of GFNE and GFNB on growth inhibition of planktonic bacteria, cell aggregation to form biofilm and cell dispersion from preformed biofilm leading to disaggregation of biofilm network

Compounds	Antibacterial concentration (µg mL^{-1})		Antibiofilm concentration (µg mL^{-1})		Minimum biofilm dispersion concentration	
	E. coli MTCC 443	*B. subtilis* MTCC 441	*E. coli* MTCC 443	*B. subtilis* MTCC 441	*E. coli* MTCC 443	*B. subtilis* MTCC 441
GFNE	3.2	4.2	0.80	1.05	1.21	2.09
GFNB	1.3	3.2	0.325	0.8	0.55	1.20

inhibition at 4.2 µg mL^{-1} (63.9%) [Fig. 2C] and 3.2 µg mL^{-1} (63.07%) [Fig. 2D], respectively. R^2 values signified the linearity of curve to express significance of percentage inhibition and maximum R^2value of GFNB on *B. subtilis* revealed that the compound had very significant effect over the entire range of concentrations studied.

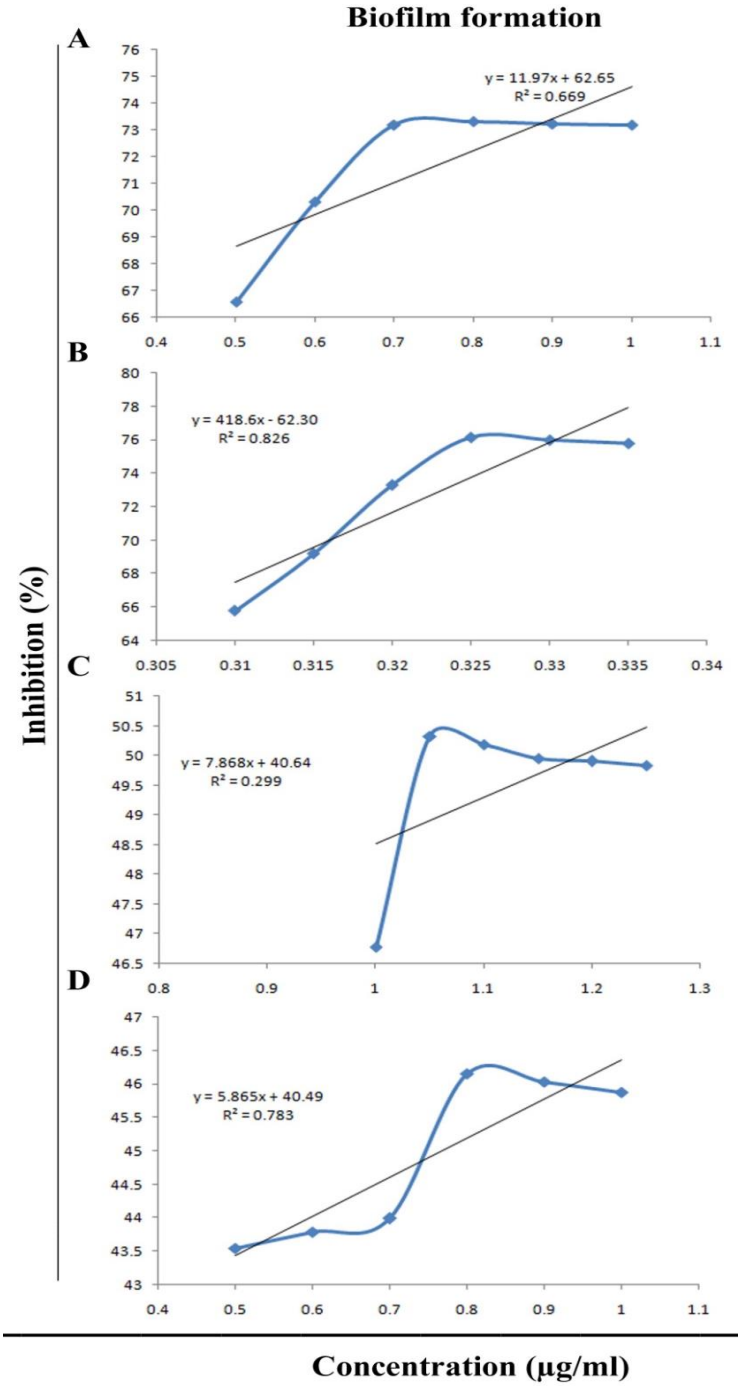

Fig 3: Effect of GFNE [2E], GFNB [2F] against *E. coli* biofilm and GFNE [2G], GFNB [2H] against *B. subtilis* biofilm are shown. Both antibacterial and antibiofilm concentrations are expressed with respect to their corresponding percentage inhibition. R^2 value shows the linearity of the curve to express significance of percentage inhibition or percentage dispersion.

Planktonic bacteria through colonization by quorum sensing aggregate into a film like network called biofilm. Further, 1/4th sub-inhibitory concentrations were chosen for antibiofilm assay to check efficiency of these concentrations on aggregation of bacteria and formation of biofilm. It was found that iron oxide NPs attenuated the aggregation of bacteria to form biofilm to the extent of 73.31% at 0.8 µg mL^{-1} and 76.15% at 0.325µg mL^{-1} by GFNE [Fig. 3A] and GFNB [Fig. 3B], respectively against *E. coli* and at 50.33% at 1.05 µg mL^{-1}, 46.15% at 0.8 µg mL^{-1} by GFNE [Fig. 3C] and GFNB [Fig. 3D], respectively against *B. subtilis*. The results revealed that FeO NPs have capability of modulating bio-film formation at their very low 1/4th sub-inhibitory concentration. R^2 value signifies the linearity of the curve to express significance of percentage inhibition in biofilm formation and maximum R^2 value of GFNB on *E. coli* showed that the compound had very significant effect over the entire range of concentrations studied for their effect on aggregation and biofilm formation. Pathologically biofilm may be formed in wounds, in dental plaques, teeth and other regions of the body. Thus it is quite relevant that at times cells have to be dislodged from the biofilm network to revert the pathology. In such cases biofilm dispersion is much essential. In present study, FeO NPs attenuated the aggregation of bacteria to form

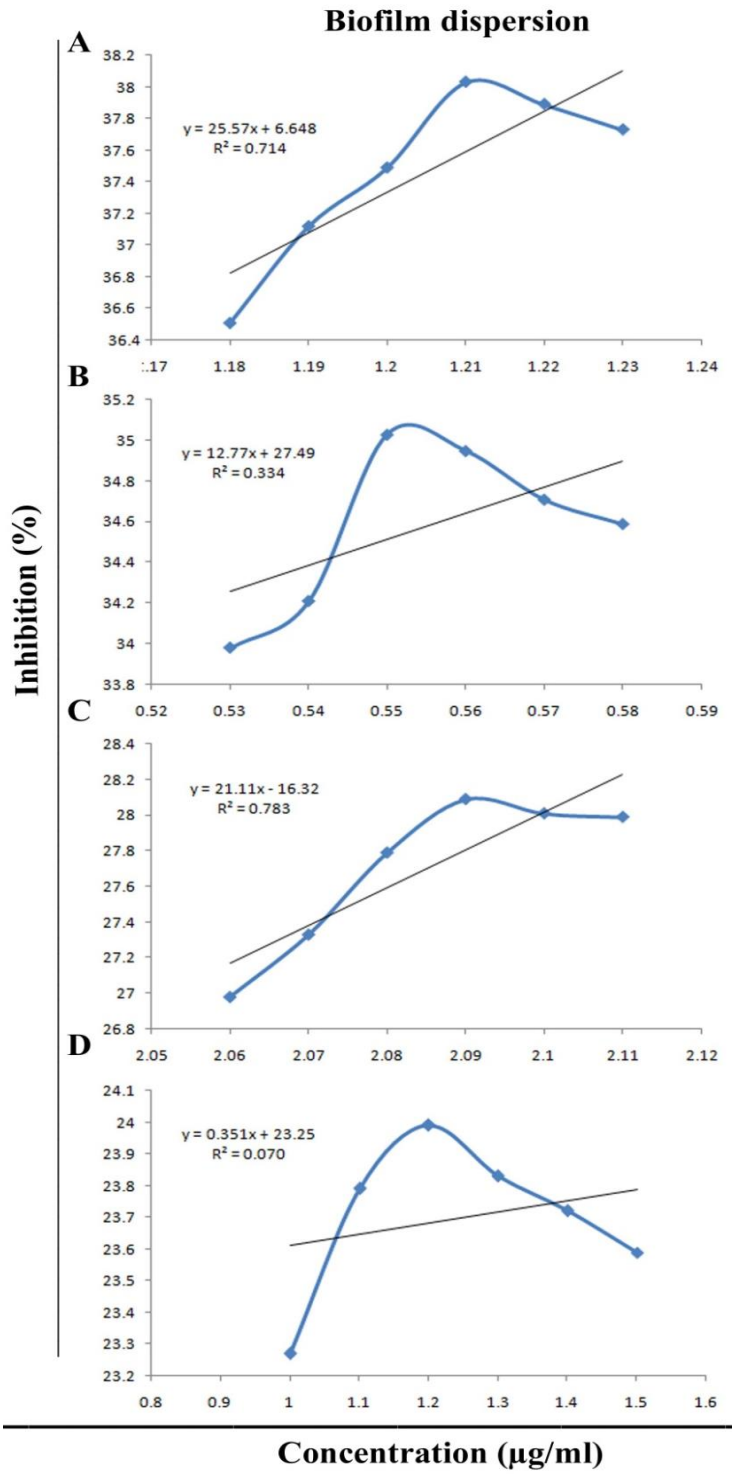

Fig. 4: Potential concentrations of GFNE [2I], GFNB [2J] in dispersing *E. coli* from biofilm and GFNE [2K], GFNB [2L] in dispersing *B. subtilis* from biofilm are shown with respect to their corresponding percentage dispersion. R^2 value shows the linearity of the curve to express significance of percentage inhibition or percentage dispersion.

biofilm at 1.21 µg mL^{-1} with 38.03% and 0.55 µg mL^{-1} with 35.03% by GFNE [Fig. 4A] and GFNB [Fig. 4B], respectively against *E. coli* and at 2.09 µg mL^{-1} with 28.09%, 1.2 µg mL^{-1} with 23.99% for GFNE [Fig. 4C] and GFNB [Fig. 4D], respectively against *B. subtilis*. This signifies that FeO NPs had moderate effect in dispersing the planktonic bacteria from biofilm to dislodge the biofilm structure [Table 1]. The maximum R^2 value of GFNE on *B. subtilis* showed that the compound had very significant effect on the entire range of concentrations studied for their effect in dispersing planktonic cells from preformed biofilm.

The aggregation of bacteria and formation of biofilm after treatment with FeO NPs were observed under fluorescent microscope. It was observed that by treatment with sub-inhibitory concentrations FeO NPs, both *E. coli* and *B. subtilis* were substantially attenuated to aggregate and form biofilm with respect to untreated control [Fig. 5]. Streptomycin was taken as reference standard to study biofilm attenuation. Attenuation in biofilm formation was observed through modulation in bacterial total protein and bacterial EPS formation. GFNE and GFNB attenuated both *E. coli* and *B. subtilis* biofilm total protein and EPS significantly [Table 2]. This signifies that GFNE and GFNB modulate *E. coli* and *B. subtilis* biofilm formation through modulation of protein content and EPS formation which leads to reduced aggregation of planktonic cells over substrates.

Ground water in the localities of Tripura contains aggregated iron oxides, sometimes dispersed as

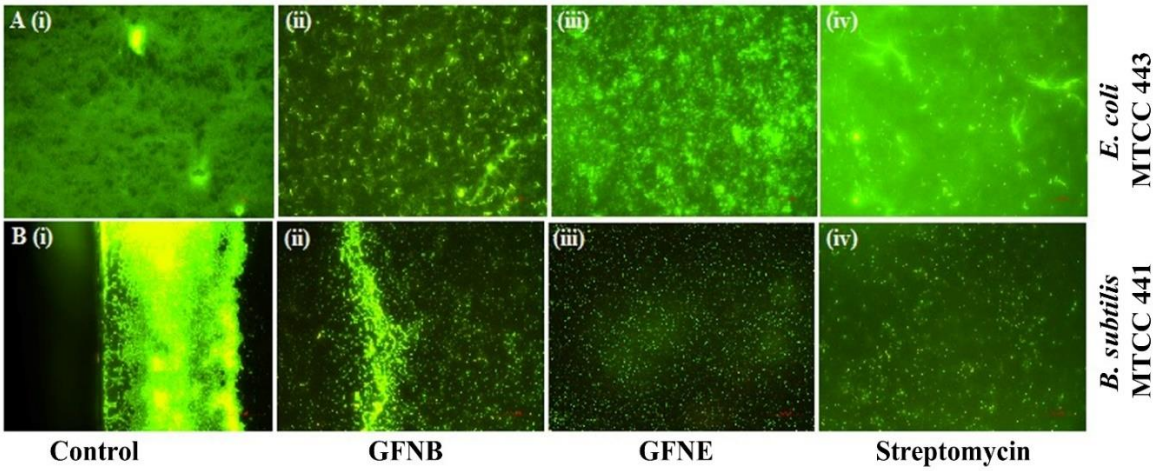

Fig. 5: Fluorescent microscopic observation of effect of sub-inhibitory concentrations of GFNB [A(ii)], [B(ii)] and GFNE [A(iii)], [B(iii)] on *E. coli* and *B. subtilis*, respectively, toward their aggregation and biofilm formation with respect to untreated control [A(i)], [B(ii)] and reference standard antibiotic streptomycin [A(iv)], [B(iv)] are shown.

Table 2: Effect of GFNE and GFNB on inhibition of *E. coli* and *B. subtilis* total protein and EPS leading to attenuation in aggregation to form biofilm network

Compounds	Bacterial total protein inhibition		Bacterial EPS inhibition	
	E. coli MTCC 443	*B. subtilis* MTCC 441	*E. coli* MTCC 443	*B. subtilis* MTCC 441
GFNE	66.27%	46.45%	69.21%	48.55%
GFNB	69.99%	43.18%	72.43%	46.97%

solution or suspension. People used to collect this ground water for drinking and other purposes. As a result, the people develop various gastro-intestinal tract associated pathological conditions. Also, these dissolved irons make water and household articles reddish yellow in colour (Mahto *et al*., 2022; Das *et al*., 2022). In present study a successful attempt has been made to convert these dissolved or suspended iron oxides into nanoparticles and explore its beneficial effect.

Bacteria in planktonic architecture exist as free unbound entity in nature. From these state planktonic cells communicate with each other through quorum sensing to become aggregated. Through quorum sensing the cells produce EPS membrane upon which planktonic cells embed themselves to form network like structure called biofilm. In present study, *E. coli* and *B. subtilis* were grown in culture and allowed to develop biofilm embedded through EPS membrane. Such EPS were collected and used as reducing agent to convert iron from groundwater into nanoparticles through hydrothermal method. This method is a very substantial method where moist heat (120C) is applied under 15 psi pressure in presence of reducing agent (Parulekar *et al*., 2019; Rashid *et al*., 2021). The EPS membrane acts as reducing agent to reduce iron oxides in nanoparticles. The syntheses of uncoloured NPs were confirmed through presence of peaks in UV range observed through UV spectrophotometer (Poulose *et al*., 2014). IR spectroscopy confirms the presence of functional groups in the synthesized NPs through presence of peaks specific bandwidths (Mudunkotuwa *et al*., 2014). Further, XRD analysis confirms that NPs produced utilizing EPS of both bacteria are crystalline in nature with face centred cubic (FCC) structure. In addition, TEM and selected area electron diffraction (SAED) study confirmed that both NPs were pure crystalline in nature with very small < 5 nm in particle size. This signifies that the hydrothermal method utilizing bacterial EPS have converted the dissolved and suspended iron into small crystalline NPs which were converted into uncoloured from reddish yellow colour (Tetyczka *et al*., 2019; Petrushevska *et al*., 2019).

Both GFNB and GFNE executed attenuation of *B. subtilis* and *E. coli* at < 5 µg mL^{-1} concentration. Effect of these NPs on cellular aggregation and biofilm formation were studied at sub-

inhibitory concentrations. The 1/4th sub-inhibitory concentration of both NPs executed significant attenuation in bacterial aggregation to form biofilm. At certain sub-inhibitory concentration, these NPs started dispersing planktonic cells from biofilm to dislodge the network architecture. In expressing result of antibacterial and antibiofilm, R^2 value expressed linearity of data plotted in the curve and the significance of data in the series of concentrations that were studied. The effects of NPs on biofilm network were also observed under fluorescent microscope with respect to untreated control and streptomycin as reference antibiotic.

Conclusion: The present study explored the potential of bacterial EPS mediated hydrothermal technique in converting ground water iron into nanoparticles. Size, shape and morphology of NPs were identified through characterisation. The synthesized NPs showed significant effect on planktonic bacterial growth, aggregation of planktonic cells to form biofilm network and dispersion of calls from preformed biofilm. In a nutshell the study explores bacterial EPS mediated reduction into NPs and execution of anti-biofilm effect by produced NPs.

Acknowledgements: Authors acknowledge the Women's Polytechnic, Hapania, Tripura, India for providing instrumental and chemical support to complete the work. Authors also thank SAIF, NEHU, Shillong, Meghalaya, India, Dept. of Molecular Biology & Bioinformatics, Tripura University, India and State Biotech Hub, Tripura, India for extending their instrumental support to complete the work.

Conflict of interest: Authors have declared that they have no conflicts of interest.

Authors' contribution: MCD designed the experimental set up, while RD, SB and MCD performed all the experiments. DB and MCD performed data analysis and graphical representation of data while LRS extended high end instrumental support and analysed the data along with RD. AB, DB and MCD compiled all data and prepared the manuscript.

REFERENCES

Armbruster, C.R., Lee, C.K., Parker-Gilham, J., de Anda, J., Xia, A., Zhao, K., *et al.,* 2019. Heterogeneity in surface sensing suggests a division of labor in *Pseudomonas aeruginosa* populations. *Elife*, **8**: e45084. [*https://doi.org/10.7554/eLife.45084*].

Bunjes, H. and Unruh, T. 2007. Characterization of lipid nanoparticles by differential scanning calorimetry, X-ray and neutron scattering. *Advanced Drug Delivery Reviews*, **59**(6): 379-402.

Bustamante-Torres, M., Romero-Fierro, D., Estrella-Nuñez, J., Arcentales-Vera, B., Chichande-Proaño, E. and Bucio, E. 2022. Polymeric composite of magnetite iron oxide nanoparticles and their application in biomedicine: A review. *Polymers*, **14**(4): 752. [*https://doi.org/10.3390/polym14040752*].

Das, M.C., Samaddar, S., Jawed, J.J., Ghosh, C., Acharjee, S., Sandhu, P., *et al.*, 2022. Vitexin alters *Staphylococcus aureus* surface hydrophobicity to obstruct biofilm formation. *Microbiological Research*, **263**: 127126. [*https://doi.org/10.1016/j.micres.2022.127126*].

Edet, U.O., Bassey, I.U. and Joseph, A.P. 2023. Heavy metal co-resistance with antibiotics amongst bacteria isolates from an open dumpsite soil. *Heliyon*, **9**(2): e13457. [*https://doi.org/10.1016/j.heliyon.2023.e13457*].

Erega, A., Stefanic, P., Dogsa, I., Danevčič, T., Simunovic, K. and Klančnik, A. 2021. Bacillaene mediates the inhibitory effect of *Bacillus subtilis* on *Campylobacter jejuni* biofilms. *Applied and Environmental Microbiol*ogy, **87**(12): e0295520. [*https://doi.org/10.1128/AEM.02955-20*].

Garza-Cervantes, J.A., Escárcega-González, C.E., Barriga Castro, E.D., Mendiola-Garza, G., Marichal-Cancino, B.A., López-Vázquez, M.A., *et al.*, 2019. Antimicrobial and antibiofilm activity of biopolymer-Ni, Zn nanoparticle biocomposites synthesized using *R.*

mucilaginosa UANL-001L exopolysaccharide as a capping agent. *International Journal of Nanomedicine*, **14**: 2557-2571.

Gobinda Dey, Patil, M.P., Banerjee, A., Sharma, R.K., Banerjee, P., Maity, J.P., *et al.*, 2023. The role of bacterial exopolysaccharides (EPS) in the synthesis of antimicrobial silver nanomaterials: A state-of-the-art review. *Journal of Microbiological Methods*, **212**: 106809. [*https://doi.org/10.1016/j.mimet.2023.106809*].

Grégorio, C., Harmel, N.P., Frédéric, G. and Capucine, R. 2007. Removal of C.I. basic green 4 (malachite green) from aqueous solutions by adsorption using cyclodextrin-based adsorbent: Kinetic and equilibrium studies. *Seperation and Purification Technology*, **53**(1): 97-110.

Jacinto, M.J., Silva, V.C., Valladão, D.M.S. and Souto, R.S. 2021. Biosynthesis of magnetic iron oxide nanoparticles: A review. *Biotechnology Letters*, **43**(1): 1-12.

Kobayashi, T., Ikeda, M., Okada, Y., Higurashi, Y., Okugawa, S. and Moriya, K. 2021. Clinical and microbiological characteristics of recurrent *Escherichia coli* bacteremia. *Microbiology Spectrum*, **9**(3): e0139921. [*https://doi.org/10.1128/Spectrum.01399-21*].

Kibret, M. and Abera, B. 2011. Antimicrobial susceptibility patterns of *E. coli* from clinical sources in northeast Ethiopia. *African Health Sciences*, **11** (Suppl 1): S40-S45. [*https://doi.org/10.4314/ahs.v11i3.70069*].

Li, H., Liu, H., Zhang, L., Hieawy, A. and Shen, Y. 2023. Evaluation of extracellular polymeric substances matrix volume, surface roughness and bacterial adhesion property of oral biofilm. *Journal of Dental Sciences*, **18**(4): 1723-1730.

Li, J., Wang, S., Shi, X. and Shen, M. 2017. Aqueous-phase synthesis of iron oxide nanoparticles and composites for cancer diagnosis and therapy. *Advances in Colloid and Interface Sciences*, **249**: 374-385.

Mahto, K.U. and Das, S. 2022. Bacterial biofilm and extracellular polymeric substances in the moving bed biofilm reactor for wastewater treatment: A review. *Bioresource Technology*, **345**: 126476. [*https://doi.org/10.1016/j.biortech.2021.126476*].

Malhotra, M., Pal, M., Chakrabortty, S. and Pal, P. 2023. A single functionalized graphene nanocomposite in cross flow module for removal of multiple toxic anionic contaminants from drinking water. *Environmental Science Pollution Research International*, **30**(24): 65250-65266.

Miškovská, A., Rabochová, M., Michailidu, J., Masák, J., Čejková, A., Lorinčík, J., *et al.*, 2022. Antibiofilm activity of silver nanoparticles biosynthesized using viticultural waste. *Public Library of Science One*, **17**(8): e0272844. [*https://doi.org/10.1371/journal.pone.0272844*].

More, P.R., Pandit, S., Filippis, A., Franci, G., Mijakovic, I. and Galdiero, M. 2023. Silver nanoparticles: Bactericidal and mechanistic approach against drug resistant pathogens. *Microorganisms*, **11**(2): 369. [*https://doi.org/10.3390/microorganisms11020369*].

Mudunkotuwa, I.A., Minshid, A.A. and Grassian, V.H. 2014. ATR-FTIR spectroscopy as a tool to probe surface adsorption on nanoparticles at the liquid-solid interface in environmentally and biologically relevant media. *Analyst*, **139**(5): 870-881.

Nagao, Y., Koh, S., Taguchi, S. and Shimada, T. 2023. Cell-growth phase-dependent promoter replacement approach for improved poly(lactate-co-3-hydroxybutyrate) production in *Escherichia coli*. *Microbial Cell Factories*, **22**(1): 131. [*https://doi.org/10.1186/s12934-023-02143-w*].

Nagarajan, D.R. and Krishnan, C. 2010. Use of a new catabolite repression resistant promoter isolated from *Bacillus subtilis* KCC103 for hyper-production of recombinant enzymes. *Protein Expression and Purification*, **70**(1): 122-128.

Nandanwar, N., Janssen, T., Kühl, M., Ahmed, N., Ewers, C., and Wieler, L.H. 2014. Extraintestinal pathogenic *Escherichia coli* (ExPEC) of human and avian origin belonging to sequence type complex 95 (STC95) portray indistinguishable virulence features. *International Journal of Medical Microbiology*, **304**(7): 835-842.

Pandi, K., Viswanathan, N. and Meenakshi, S. 2019. Hydrothermal synthesis of magnetic iron oxide encrusted hydrocalumite-chitosan composite for defluoridation studies. *International Journal of Biological Macromolecules*, **132**: 600-605.

Parulekar, R.S., Barale, S.S. and Sonawane, K.D. 2019. Antibiotic resistance and inhibition mechanism of novel aminoglycoside phosphotransferase APH(5) from *B. subtilis* subsp. *subtilis* strain RK. *Brazilian Journal of Microbiology*, **50**(4): 887-898.

Petrushevska, M., Pavlovska, K., Laskova, J., Zdravkovski, P. and Dodov, M.G. 2019. Transmission electron microscopy: Novel application of established technique in characterization of nanoparticles as drug delivery systems. *Prilozi (Makedon Akad Nauk Umet Odd Med Nauki)*, **40**(2): 67-72.

Poulose, S., Panda, T., Nair, P.P. and Théodore, T. 2014. Biosynthesis of silver nanoparticles. *Journal of Nanoscience and Nanotechnology*, **14**(2): 2038-2049.

Qin, Q., Olimov, D. and Yin, L. 2022. Semiconductor-type gas sensors based on γ-Fe_2O_3 nanoparticles and its derivatives in conjunction with SnO_2 and graphene. *Chemosensors*, **10**(7): 267. [*https://doi.org/10.3390/chemosensors10070267*].

Raeispour, M. and Ranjbar, R. 2018. Antibiotic resistance, virulence factors and genotyping of uropathogenic *Escherichia coli* strains. *Antimicrobial Resistance and Infection Control*, **7**: 118. [*https://doi.org/10.1186/s13756-018-0411-4*].

Rashid, M., Rabbi, M.A., Ara, T., Hossain, M.M., Islam, M.S., Elaissari, A., *et al.*, 2021. Vancomycin conjugated iron oxide nanoparticles for magnetic targeting and efficient capture of Gram-positive and Gram-negative bacteria. *RSC Advances*, **11**(57): 36319-36328.

Reddy, P.M., Chang, K.C., Liu, Z.J., Chen, C.T. and Ho, Y.P. 2014. Functionalized magnetic iron oxide (Fe_3O_4) nanoparticles for capturing Gram-positive and Gram-negative bacteria. *Journal of Biomedical Nanotechnology*, **10**(8): 1429-1439.

Saravanakumar, K., Sathiyaseelan, A., Manivasagan, P., Jeong, M.S., Choi, M., Jang, E.S., *et al.*, 2022. Photothermally responsive chitosan-coated iron oxide nanoparticles for enhanced eradication of bacterial biofilms. *Biomaterials Advances*, **141**: 213129. [*https://doi.org/10.1016/j.bioadv.2022.213129*].

Scala, A., Piperno, A., Hada, A., Astilean, S., Vulpoi, A., Ginestra, G., *et al.*, 2019. Marine bacterial exopolymers-mediated green synthesis of noble metal nanoparticles with antimicrobial properties. *Polymers*, **11**(7): 1157. [*https://doi.org/10.3390/polym11071157*].

Swidan, N.S., Hashem, Y.A., Elkhatib, W.F. and Yassien, M.A. 2022. Antibiofilm activity of green synthesized silver nanoparticles against biofilm associated enterococcal urinary pathogens. *Scientific Reports*, **12**(1): 3869. [*https://doi.org/10.1038/s41598-022-07831-y*].

Tetyczka, C., Hodzic, A., Kriechbaum, M., Juraić, K., Spirk, C., Hartl, S., *et al.*, 2019. Comprehensive characterization of nanostructured lipid carriers using laboratory and synchrotron X-ray scattering and diffraction. *European Journal of Pharmaceutics and Biopharmaceutics*, **139**: 153-160.

Traub, W.H., Leonhard, B. and Bauer, D. 1998. Antibiotic susceptibility of *Stenotrophomonas* (*Xanthomonas*) *maltophilia*: Comparative (NCCLS criteria) evaluation of antimicrobial drugs with the agar dilution and the agar disk diffusion (Bauer-Kirby) tests. *Chemotherapy*, **44**(3): 164-173.

Yadwade, R., Kirtiwar, S. and Ankamwar, B. 2021. A review on green synthesis and applications of iron oxide nanoparticles. *Journal of Nanoscience and Nanotechnology*, **21**(12): 5812-5834.

Yasemin, B. and Haluk, A. 2006. A kinetics and thermodynamics study of methylene blue adsorption on wheat shells. *Desalination*, **194**(1-3): 259-267.